2021

Photodegradation of reactive blue 19 dye using magnetic nanophotocatalyst α-Fe2O3/WO3: A comparison study of α-Fe2O3/WO3 and WO3/NaOH

Mohammad Delnavaz

Javad Farahbakhsh
Edith Cowan University

Seyed Sajad Mahdian

10.1016/j.wse.2021.06.007
Delnavaz, M., Farahbakhsh, J., & Mahdian, S. S. (2021). Photodegradation of reactive blue 19 dye using magnetic nanophotocatalyst α-Fe2O3/WO3: A comparison study of α-Fe2O3/WO3 and WO3/NaOH. *Water Science and Engineering, 14*(2), 119-128.https://doi.org/10.1016/j.wse.2021.06.007

Water Science and Engineering 2021, 14(2): 119−128

HOSTED BY

ELSEVIER

Available online at www.sciencedirect.com

Water Science and Engineering

journal homepage: wse.hhu.edu.cn

Photodegradation of reactive blue 19 dye using magnetic nanophotocatalyst α-Fe_2O_3/WO_3: A comparison study of α-Fe_2O_3/WO_3 and WO_3/NaOH

Mohammad Delnavaz [a,*], Javad Farahbakhsh [b], Seyed Sajad Mahdian [a]

[a] *Civil Engineering Department, Faculty of Engineering, Kharazmi University, Tehran 15719-14911, Iran*
[b] *School of Engineering, Edith Cowan University, Joondalup WA 6027, Australia*

Received 24 October 2020; accepted 5 February 2021
Available online 19 June 2021

Abstract

The photocatalytic degradation of reactive blue 19 (RB19) dye was investigated in a slurry system using ultraviolet (UV) and light-emitting diode (LED) lamps as light sources and using magnetic tungsten trioxide nanophotocatalysts (α-Fe_2O_3/WO_3 and WO_3/NaOH) as photocatalysts. The effects of different parameters including irradiation time, initial concentration of RB19, nanophotocatalyst dosage, and pH were examined. The magnetic nanophotocatalysts were also characterized with different methods including scanning electron microscopy (SEM), energy-dispersive X-ray spectroscopy (EDS), transmission electron microscopy (TEM), X-ray diffraction (XRD), photoluminescence (PL), differential reflectance spectroscopy (DRS), Fourier transform infrared spectroscopy (FTIR), and vibrating sample magnetometry (VSM). The XRD and FTIR analyses confirmed the presence of tungsten trioxide on the iron oxide nanoparticles. The VSM analysis confirmed the magnetic ability of the new synthesized nanophotocatalyst α-Fe_2O_3/WO_3 with 39.6 emu/g of saturation magnetization. The reactor performance showed considerable improvement in the α-Fe_2O_3-modified nanophotocatalyst. The impact of visible light was specifically investigated, and it was compared with UV-C light under the same experimental conditions. The reusability of the magnetic nanophotocatalyst α-Fe_2O_3/WO_3 was tested during six cycles, and the magnetic materials showed an excellent removal efficiency after six cycles, with just a 7% decline.

Keywords: Reactive blue 19; Magnetic nanophotocatalyst; α-Fe_2O_3/WO_3; Saturation magnetization; UV-C lamps

1. Introduction

Textile manufacturing is an important industry generating different materials for use in the production of rugs, clothes, tablecloths, car seat upholstery, and chair upholstery. Due to its wide application in various areas, determination of the environmental consequences of textile manufacture is vital. At different stages of the textile industry, huge amounts of water and chemical substances are consumed. The generated wastewater at these stages can pose serious threats to both the environment and human health (Kabra et al., 2013; Kansal et al., 2007). Textile wastewater is regarded as one of the most harmful types of sewage due to its discharge rate and its composition. In fact, textile wastewater introduces a wide range of organic pollutants into water resources (Lourenço et al., 2015; Yurtsever et al., 2016). It is estimated that wastewater contains large quantities of dyes (approximately 10%−15%), which should be degraded with available treatment techniques. Discharging untreated dye wastewater into water bodies is potentially destructive to the environment because of the reduction of sunlight exposure on the water surface, eutrophication, and water ecological intervention.

Degradation of dyes is highly complicated and time-consuming. In order to degrade these materials from water or wastewater, conventional methods, such as adsorption (Pirkarami and Olya, 2017), membrane filtration (Marcucci

The work was supported by the Fund of Kharazmi University (Grant No. 22073).
* Corresponding author.
E-mail address: delnavaz@khu.ac.ir (Mohammad Delnavaz).
Peer review under responsibility of Hohai University.

https://doi.org/10.1016/j.wse.2021.06.007

et al., 2001), and coagulation (Al-Ani and Li, 2012), have been studied. These techniques not only impose economic costs and operational burdens on treatment processes, but also convert biodegradable materials into sludge and produce a new type of contaminants requiring further purification (Guimarães et al., 2012). These obstacles have caused researchers to develop and assess new dye degradation methods.

As one of the advanced oxidation processes, the photocatalytic process has been recently investigated by many scientists around the world. Novel photocatalysts can easily complete the mineralization of organic matter without posing any threats to the environment or human health (Bel Hadjltaief et al., 2019). Of the different semiconductors used in photocatalytic processes, TiO_2 is the most common owing to its reactivity, low cost, and wide energy gap (Chen and Poon, 2009). However, the large energy gap (3.23 eV), the high rate of electron−hole recombination, and the complicated separation process decrease the efficiency of TiO_2. Therefore, other semiconductors, such as inorganic semiconductor heterostructures, WO_3 with different composite forms including WO_3 nanorods, WO_3 loaded with NaOH, magnetic tungsten trioxide (Fe_3O_4/WO_3), and ZnO composites, including magnetic zinc sulfide, ZnO/TiO_2 thin-film photocatalysts, and magnetic hybrid ZnO photocatalysts with lower band gaps and mechanisms for easier separation, have been widely used in recent studies (Abbasi Asl et al., 2020; Gómez-Pastora et al., 2017; Karimi et al., 2020; Mkhalid, 2016; Parthibavarman et al., 2018; Serrà et al., 2020). WO_3 nanocomposites with low band gaps (2.4−2.7 eV) are considered a powerful candidate for photocatalytic processes because of their high adsorption capacity and thermal and physical stability within the visible light spectrum (Han et al., 2016; Kako et al., 2014). Mu et al. (2017) used WO_3 coated with Fe_3O_4 as a magnetic photocatalyst to remove Cs^+ and Sr^{2+} from aqueous solution and found that the synthesized magnetic nanoparticles have the best adsorption capacities, 44.178 and 53.175 mg/g for Sr^{2+} and Cs^+, respectively. Kako et al. (2014) investigated the improvement of WO_3 with NaOH and found that photocatalytic activity increased 120 times beyond that associated with pure WO_3 when just 5% of NaOH was loaded on the surface of WO_3. The application of inorganic semiconductor heterostructures is considered an effective strategy for the degradation of different pollutants. Inorganic semiconductors such as TiO_2, ZnO, and WO_3 are strong photocatalysts in degradation processes due to redox reactions created by photo-generated electron−hole pairs. With regard to the recent attempts using inorganic semiconductor heterostructures, Zhang et al. (2017) used new $Ag/AgGaO_2$ metal semiconductor heterostructures (MSH) to degrade methylene blue, and the new photocatalyst showed an excellent photocatalytic ability, degrading up to 95% of methylene blue, which was 31.2% more than what a pure $AgGaO_2$ photocatalyst was able to degrade. For bacterial elimination, Hong et al. (2019) used $Bi_2S_3@Ag_3PO_4/Ti$ in inorganic semiconductor heterostructures to remove *Staphylococcus aureus* and *Escherichia coli*, and the new photocatalyst performed well in photocatalysis and photothermal effects against these bacteria with a removal efficiency of up to 95%. Wang et al. (2018) used the $FeWO_4/Fe_2O_3$ di-modified WO_3 photocatalyst to remove quasi-phenothiazine dyes such as methylene blue, toluidine blue, azure I, and acridine orange under visible light irradiation; the synthetic process was implemented with a one-step method; the presence of $FeWO_4$ and α-Fe_2O_3 clusters efficiently reduced the recombination rate; and the results showed a high removal efficiency for these dyes. There have been many other recent studies regarding inorganic semiconductor heterostructures, which have shown unprecedented results compared to other semiconductors (Hitkari et al., 2018; Hosseini et al., 2014; Li et al., 2016). Therefore, using these structures can be effective in photocatalytic processes, especially dye degradation.

One of the main challenges in photocatalytic processes is the separation mechanism. It is always difficult to remove photocatalysts after the degradation process (Banić et al., 2019). The use of magnetic materials has shown a significant improvement in the separation process. Using magnetic materials as photocatalysts facilitates the separation process with the aid of an external magnetic field. In addition, the recycling of nanophotocatalysts becomes much easier when magnetic materials are used in the photocatalyst structure. Banić et al. (2019) studied the separation mechanism using Fe_3O_4/WO_3 as a magnetic nanophotocatalyst and enhanced the magnetic separation process through the coupling of WO_3 and Fe_3O_4; the use of 1.4% of WO_3 with Fe_3O_4 increased the separation efficiency up to 58% under an external magnetic field of 160 mT. Although magnetic photocatalysts have performed well in photocatalytic processes, more research is still needed. Given that many studies have merely focused on the magnetic photocatalysts based on TiO_2, other semiconductors combined with magnetic materials needed to be fully investigated (Gómez-Pastora et al., 2017; Xue et al., 2019).

In this study, magnetic α-Fe_2O_3/WO_3 was used as a new magnetic photocatalyst in the dye degradation process. A comparison between WO_3/NaOH and α-Fe_2O_3/WO_3 was also conducted under the irradiation of ultraviolet (UV) and visible light-emitting diode (LED) lamps. Recently, there have been few studies of the photodegradation of organic pollutants under different conditions with the aid of α-Fe_2O_3/WO_3. Magnetic materials are critical for the separation of pollutants from wastewater, especially in slurry systems. Therefore, this study tested these synthesized magnetic materials under different conditions in comparison with common WO_3/NaOH composites, and their performance and behavior in photocatalytic processes were investigated.

2. Materials and methods

2.1. Materials

The commercial name of reactive blue 19 dye (RB19) (general formula: $C_{22}H_{16}N_2Na_2O_{11}S_3$) is remazol brilliant

blue, and its functional group is anthraquinone. In this study, the molecular mass and purity of RB19 were 626.54 g/mol and 99%, respectively. The photocatalyst used in this study was WO_3, which was manufactured by the Western Minmetals (SC) Corporation, in China. Ferric chloride, sodium hydroxide, and ammonia solution were prepared by Sigma−Aldrich Inc.

2.2. Characterization

The properties of WO_3/NaOH and magnetic α-Fe_2O_3/WO_3 were well described by X-ray diffraction (XRD) patterns and scanning electron microscopy (SEM) analysis. The Fourier transform infrared spectroscopy (FTIR) analysis confirmed the presence of α-Fe_2O_3 on the surface of WO_3 nanoparticles. The surface morphology of the magnetic nanophotocatalyst was determined through SEM (Tescan, Czech Republic). The magnetic analysis was conducted with a vibrating sample magnetometry (VSM) device called LBKFB from Tamad Kala, produced by the Magnetic Kavir Kashan Company. VSM proved the magnetic ability of α-Fe_2O_3/WO_3 for the separation process. An ABB Bomem FTIR spectrometer (MB-104) was used for FTIR analysis. The XRD patterns were measured by an XRD device called the Rigaku Ultima IV X-ray diffractometer, at a scanning angle ranging from 10° to 60°.

2.3. Synthetic process

2.3.1. Synthesis of WO_3/NaOH

According to Kako et al. (2014), WO_3 loaded with NaOH can be more photocatalytic and positively affects the experimental results. The synthesis of WO_3/NaOH was performed through the following procedure. 10 mL of NaOH solution was added to 4 g of WO_3 powder and mixed with a stirrer for approximately 30 min. Subsequently, the solution was dried at 343 K for approximately 4−5 h. Finally, the WO_3/NaOH sample was acquired with a weight ratio of NaOH to WO_3 of 5%, and used for experiments.

2.3.2. Synthesis of α-Fe_2O_3

α-Fe_2O_3 was prepared through the co-precipitation method. First, 15 g of $FeCl_3 \cdot 6H_2O$ was dissolved in 200-mL water, and they were stirred at room temperature. 3 mL of ammonia (NH_4OH) solution was added dropwise to the solution. pH was kept constant during the synthetic process. The resulting black solution was stirred for 1 h. Subsequently, it was heated to 90°C for 2 h to evaporate all the remaining materials. The product was cooled and finally calcined at 550°C for 4 h. The resulting α-Fe_2O_3 powder was ready for use in the synthetic process described below.

2.3.3. Synthesis of α-Fe_2O_3/WO_3 composite

The magnetic α-Fe_2O_3/WO_3 nanophotocatalyst was prepared through the wet chemical process at low temperature. 70 mg of WO_3 was added to 35 mL of deionized water during ultra-sonication. 10-mg α-Fe_2O_3 and 0.20-mmol urea were added to the solution containing WO_3 and deionized water. Afterwards, the obtained mixture was continuously stirred at 40°C for 90 min. Finally, the resulting solution was centrifuged at 2 500 rpm and then washed with ethanol several times.

2.4. Apparatus and sampling procedure

The volume of the reactor was 200 mL in batch mode. The feeding synthetic wastewater was prepared in the range of 10−20 mg/L by dissolving RB19. In order to achieve complete mixing and prevent nanophotocatalyst deposition from occurring, a magnetic stirrer was placed at the bottom of the reactor. UV-C and LED lamps provided radiation sources. The UV-C lamps (manufactured in China) emitting at 253.7 nm with a nominal power of 15 W were located inside the photo reactor, covered by aluminum foil to avoid radiation dispersion. To simulate visible light, 24 LED lamps, with an intensity of 6 100 lx, were used to monitor photocatalytic performance. The reactor setup is shown in Fig. 1.

After creation of a solution of color with the desired concentrations, the solution was placed in an ultrasonic bath (Fungilab UE-6SFD) for 10 min. The samples were then placed inside the reactor and on a magnetic stirrer to be completely mixed and prevent the sedimentation of nanophotocatalyst from occurring. The time interval for the samples was 30 min. Afterwards, the samples were centrifuged, and the remaining pollutants were quantified with a spectrophotometer (DR3900) at 590 nm. To control the accuracy of the spectrophotometer, the calibration curve was plotted every week. The wavelength of maximum absorption was 590 nm.

To study the removal efficiency, graphs were plotted showing residual color to the initial color versus time, in accordance with Eq. (1):

$$R = \left(1 - \frac{C}{C_0}\right) \times 100\% \tag{1}$$

where R is the removal efficiency, C_0 is the initial concentration (mg/L), and C is the concentration in the refined sewage at a different time (mg/L).

3. Results and discussion

3.1. Characterization of magnetic nanophotocatalyst

Based on the SEM analysis, the particle size of WO_3 nanoparticles was estimated to be 23−65 nm. Fig. 2 clearly displays the microsphere structure of α-Fe_2O_3 and α-Fe_2O_3/WO_3. As shown in Fig. 2(c), the spherical α-Fe_2O_3 was evenly dispersed on the surface of WO_3 nanoparticles. According to the SEM results, the particle size of α-Fe_2O_3/WO_3 was larger than that of α-Fe_2O_3 nanoparticles. Moreover, the surface of α-Fe_2O_3/WO_3 nanoparticles was rougher than that of WO_3 and α-Fe_2O_3 nanoparticles, which confirmed the higher stability of the new magnetic nanoparticles achieved by anchoring WO_3 on the surface of α-Fe_2O_3. The energy-

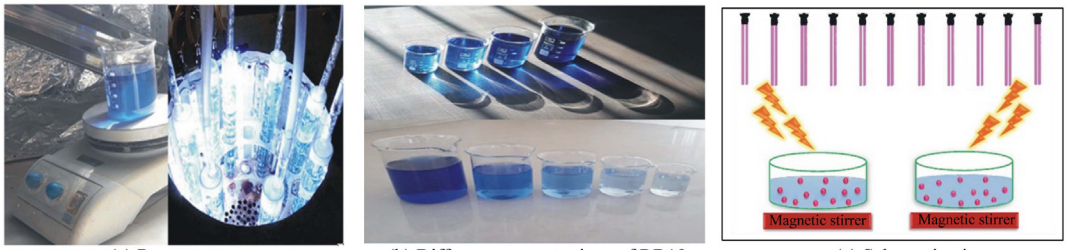

(a) Reactor setup (b) Different concentrations of RB19 (c) Schematic view

Fig. 1. Photocatalytic process of RB19 under UV and LED irradiation sources.

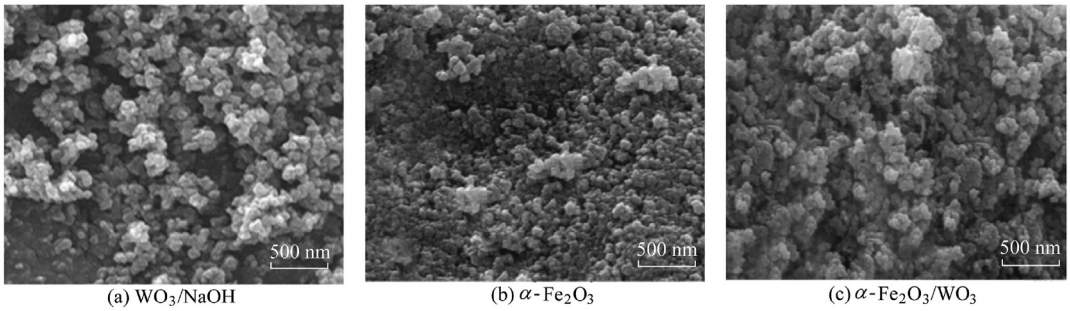

(a) WO_3/NaOH (b) α-Fe_2O_3 (c) α-Fe_2O_3/WO_3

Fig. 2. SEM analyses of WO_3/NaOH, α-Fe_2O_3, and α-Fe_2O_3/WO_3.

dispersive X-ray spectroscopy (EDS) and mapping analyses confirmed the presence of all elements in nanocomposites, including W, Fe, and O. WO_3 nanoparticles and α-Fe_2O_3 were well connected, because the weight ratio in the EDS analysis fully described the distribution of elements in the synthetic nanophotocatalyst.

Transmission electron microscopy (TEM) analysis was conducted to further investigate the surface structure of the nanophotocatalyst. Based on the TEM results shown in Fig. 3, α-Fe_2O_3 nanoparticles were successfully connected with WO_3 nano plates. The high-resolution transmission electron microscopy (HRTEM) analysis showed that the lattice distances of WO_3 and α-Fe_2O_3 were approximately 0.374 and 0.367 nm, respectively, which corresponded with the 020-lattice plane of WO_3 and the 012-lattice plane of α-Fe_2O_3. This adaptation between lattice parameters led to the perfect recombination of hematite and tungsten trioxide. The mapping element also showed the even distribution of iron on WO_3 nano plates (Fig. 3(e) and (f)).

The structures of α-Fe_2O_3/WO_3, WO_3/NaOH, and α-Fe_2O_3 were characterized through XRD analysis (Fig. 4). According to the XRD patterns, the highest points of WO_3/NaOH were observed at 22.7°, 23.1°, 23.6°, 24.3°, 26.6°, 28.9°, 31.9°, 33.3°, 34.2°, 42.8°, 50.3°, 53.3°, 54.8°, and 56.9°. This confirmed the monoclinic structure of WO_3 nanoparticles and O−H bonds. The highest points of α-Fe_2O_3 were at 29.5°, 35°, 42°, 53°, 56.5°, and 62°, also seen in the XRD pattern of α-Fe_2O_3/WO_3 magnetic nanocomposite. Moreover, the WO_3 peaks were present in the α-Fe_2O_3/WO_3 pattern, showing the strong structure of magnetic nanocomposites, both α-Fe_2O_3 and WO_3 compounds. There was no impurity in the structure of α-Fe_2O_3/WO_3 according to the XRD pattern.

The FTIR analysis also confirmed the results of XRD patterns. Fig. 5 clearly shows that the molecular structure of both α-Fe_2O_3 and WO_3/NaOH was found in the magnetic α-

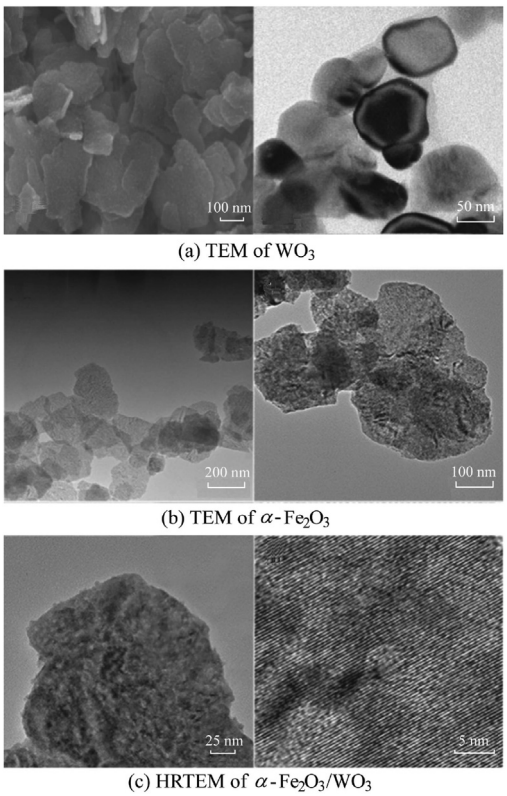

(a) TEM of WO_3

(b) TEM of α-Fe_2O_3

(c) HRTEM of α-Fe_2O_3/WO_3

Fig. 3. TEM analysis of WO_3 and α-Fe_2O_3/WO_3 and HRTEM analysis of α-Fe_2O_3/WO_3.

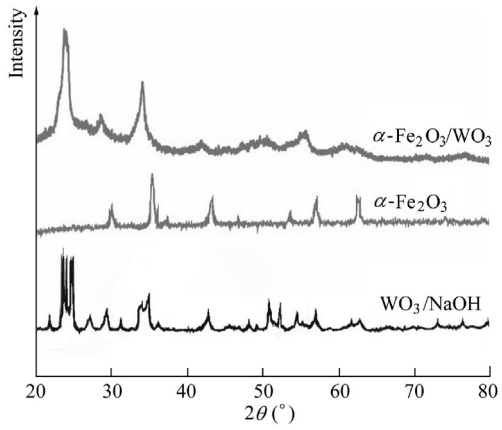

Fig. 4. XRD patterns of WO_3/NaOH, α-Fe_2O_3, and α-Fe_2O_3/WO_3 nanoparticles.

Fe_2O_3/WO_3 nanocomposite. Based on the FTIR analysis of WO_3/NaOH, the two main peaks at 800 and 940 cm^{-1} showed the stretching vibrations of W−O bonds (O−W−O stretching bonds). The bending vibrations of O−W−O occurred at 250 cm^{-1}. Moreover, O−H bonds occurred at wavenumbers of 3 000−3 500 cm^{-1}, which are not visible in the proposed range in Fig. 5. On the other side, the peaks of α-Fe_2O_3 nanoparticles at 240, 300, 430, 500, 610, 660, and 840 cm^{-1} confirmed the bending and stretching vibrations of Fe−O bonds. According to the FTIR analysis of α-Fe_2O_3/WO_3, all the aforementioned peaks also appeared in the new synthesized magnetic nanophotocatalyst. The W−O and Fe−O bonds were seen in the structure of the α-Fe_2O_3/WO_3 nanophotocatalyst (Fig. 5). These results indicated that WO_3 was successfully connected with α-Fe_2O_3 bonds, and the synthetic process has been accomplished perfectly. The existence of W−O and Fe−O bonds in the new synthesized nanocomposite with indicative peaks demonstrates the strong reaction of tungsten with Fe molecules.

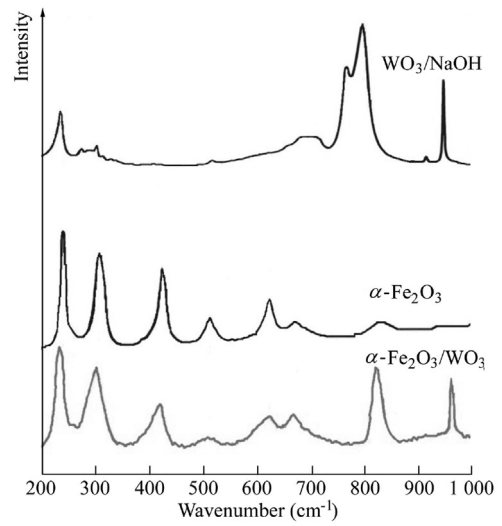

Fig. 5. FTIR analysis of WO_3/NaOH, α-Fe_2O_3, and α-Fe_2O_3/WO_3.

The magnetic behavior of the synthesized α-Fe_2O_3/WO_3 nanophotocatalyst was measured with a VSM in an external magnetic field from −10 000 to 10 000 Oe. The magnetic result of the sample was compared with that of α-Fe_2O_3 nanoparticles (Fig. 6). According to the results, the magnetic saturation values of α-Fe_2O_3/WO_3 and α-Fe_2O_3 were 39.6 and 51.2 emu/g, respectively. The presence of WO_3 particles covering α-Fe_2O_3 nanoparticles can be considered a major cause for the reduction of magnetic properties of the synthesized magnetic nanophotocatalyst. However, α-Fe_2O_3/WO_3 nanoparticles show significant magnetic behavior with a saturation magnetization value of nearly 40 emu/g. This facilitated the separation process of magnetic nanoparticles after the degradation process.

PL measurement was used to characterize the optoelectronic properties of semiconductors. The electrons were excited from the valence band to the conductance band of the material with a laser with an energy amount larger than the band gap. The photo-excited carriers could then relax and spontaneously recombine with holes in the conduction band. In the case of direct semiconductors, the excess energy was emitted in the form of light (spontaneous emission). Here, PL measurements were used to compare the recombination rate of the new nanophotocatalyst with WO_3 and hematite. The results showed that the α-Fe_2O_3/WO_3 peak decreased in comparison with those of WO_3 and α-Fe_2O_3. This reveals that the synthesized nanocomposite significantly reduced the recombination rate of WO_3 owing to the synergistic effects of α-Fe_2O_3 anchored on WO_3 nano plates. Fig. 7(a) shows the PL analysis for the studied materials.

Differential reflectance spectroscopy (DRS) analysis was used to calculate the band gap. For this purpose, the absorption spectra curve was plotted in terms of wavelength (Fig. 7(b)). The maximum slope of the tangent line to the curve and its intersection with the wavelength axis indicates the appropriate wavelength in each sample. According to the results, the band gap decreased from 2.8 eV for WO_3 to 2.4 eV for the α-Fe_2O_3/WO_3 nanocomposite. As can be seen, the synthesis reduces the band gap. Therefore, less energy is required to stimulate electron transfer from the capacity band to the conduction band. As the band gap decreases, the distance between the

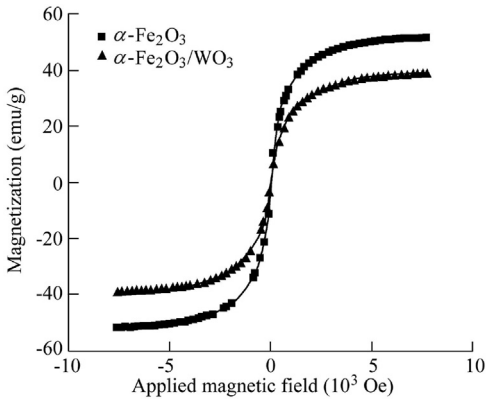

Fig. 6. VSM results of α-Fe_2O_3/WO_3 and α-Fe_2O_3.

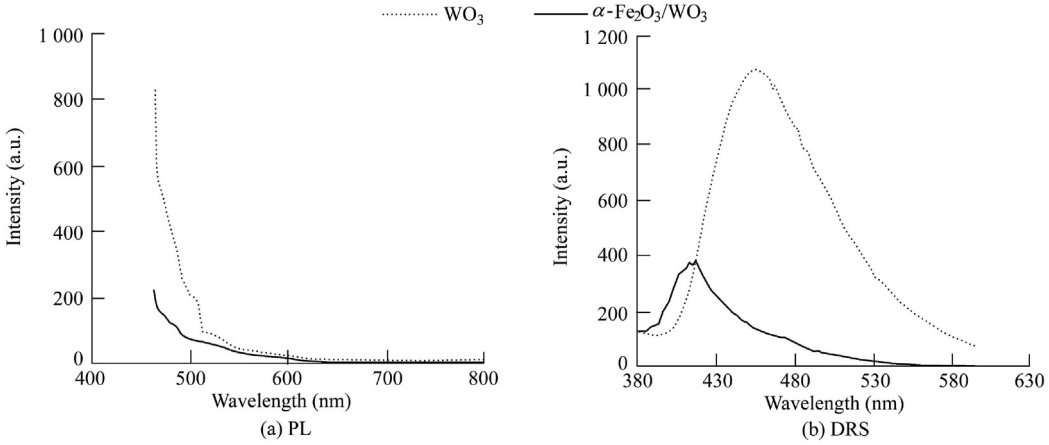

Fig. 7. PL measurement and DRS data for WO_3 and α-Fe_2O_3/WO_3 (a.u. means arbitrary units).

levels decreases, with less electron excitation energy. Clearly, the reduction of the nanocomposite band gap increases electron excitation and provides greater removal ability during irradiation.

3.2. Photodegradation of reactive blue dye with magnetic nanophotocatalyst under different conditions

3.2.1. Effect of pH

The effect of pH variations (2.0, 4.5, 7.0, and 9.5) on the removal of RB19 (30 mg/L) was investigated with irradiation time of 4 h and α-Fe_2O_3/WO_3 dosage of 1 g/L. In order to evaluate the effect of pH on the efficiency of the degradation system, the point of zero charge, the pH at which the net charge of total particle surface is equal to zero (pH_{pzc}), should be specified. At pH_{pzc}, the material surface is neutral and does not have any electrical charge. The pH_{pzc} for WO_3 has been reported to be in the range of 4−5, and α-Fe_2O_3/WO_3 also falls within this range (Manceriu and Carcel, 2011). The surface of the material is positively charged when pH is lower than pH_{pzc}, and negatively charged when the pH is higher than pH_{pzc}. Hence, the adsorption of pollutants with a positive charge occurs when the pH is higher than pH_{pzc}, and the adsorption of negatively charged pollutants occurs when the pH is lower than pH_{pzc}. Given that RB19 is in an anionic color, its absorption is higher on the surface of WO_3 when the pH is lower than 4. In this study, the highest removal efficiency of reactive blue color was observed at a pH value of 2. Fig. 8 shows the removal efficiencies of the dye. As the pH increased, the removal efficiency sharply decreased. The removal efficiencies of RB19 under the conditions of 4-h irradiation and pH values of 2.0, 4.5, 7.0, and 9.5 were 83%, 40%, 38%, and 66%, respectively. This indicates that it is important to estimate pH_{pzc} to find the highest efficiency in the optimum range of pH.

3.2.2. Effect of catalyst concentration

The catalyst is a major part of the photocalytic process because absorptive reactions only take place on the photocatalyst surface. The effect of different catalyst dosages (0.4, 0.7, 1.0, and 1.3 g/L) was investigated at a fixed initial color concentration of 30 mg/L and pH of 2. The amounts of magnetic photocatalysts directly influence the behavior of absorption. As shown in Fig. 9, an increase in the α-Fe_2O_3/WO_3 dosage enhances photocatalytic activity. In fact, more electrons are excited from the valence band to the conduction band with the aid of the visible LED or UV light source. The best photocalytic dosage was 1 g/L with 240-min contact time. However, the removal efficiency slightly dropped with a higher catalyst dosage (1.3 g/L). This can be attributed to the fact that an additional amount of catalyst particles may cause turbidity and therefore prevent photons from penetrating to the depth of the solution. In addition, more interactions between nanoparticles may lead to the desorption of weak-bond dye compounds from α-Fe_2O_3/WO_3, leading to a decrease in the removal efficiency of nanoparticles (Akyol and Bayramoğlu, 2005; Daneshvar et al., 2004). The optimum pH and photocatalyst dosage of WO_3/NaOH were also separately measured with the same irradiation time. According to the test results, the best pH was 3, and the optimum photocatalyst dosage was between 0.9 and 1.0 g/L.

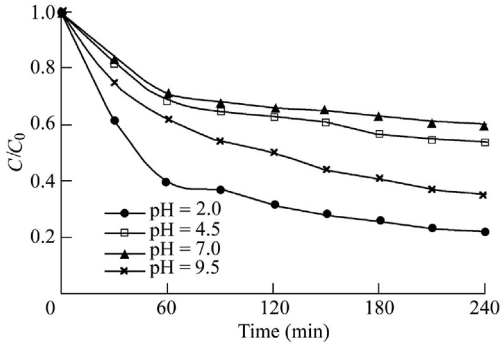

Fig. 8. Effects of contact time and primary pH on ratio of residual color to initial color (with C_0 of 30 mg/L, α-Fe_2O_3/WO_3 dosage of 1 g/L, and UV-C lamp power of 15 W).

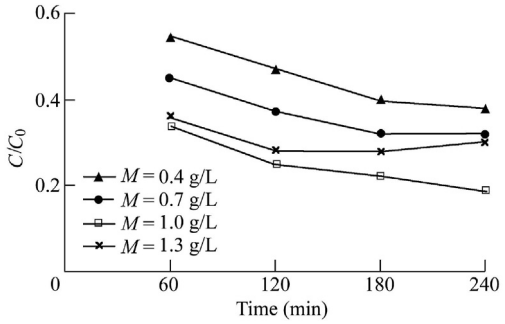

Fig. 9. Effect of catalyst concentration (M) on residual color to primary color ratio (with C_0 of 30 mg/L, initial pH of 2, and UV-C lamp power of 15 W).

3.2.3. Effect of initial dye concentration under visible LED and UV light sources with WO_3/NaOH

Under optimum conditions, the impact of two different light sources, visible LED light and UV light, on the degradation process was investigated. The degradation process was initiated with different dye concentrations of 10, 30, 50, and 70 mg/L. Other operational parameters including pH and photocatalyst dosage were fixed. The pH of the prepared solution was 2, and the catalyst dosage was fixed at 1 g/L. The exposure times for UV light and visible LED lamps were 240 and 360 min, respectively. As shown in Fig. 10(a), the dye removal efficiencies under UV-C radiation were 98%, 78%, 62%, and 51% for the initial dye concentrations of 10, 30, 50, and 70 mg/L, respectively. By contrast, when LED lamps were used, the degradation rates were 95%, 56%, 33%, and 21%, respectively. Although the irradiation time with LED lamps (360 min) was much longer than with UV-C lamps (240 min), the removal efficiencies of dye solution in the case of UV-C lamps were much higher for all initial dye concentrations. This can be attributed to the fact that the intensity of UV-C radiation is much greater than that of visible LED lamps. In this study, each LED lamp had an efficiency of up to 254 lm/W, which was lower than that of the UV-C lamp. However, the degradation process with visible light was acceptable, and it can therefore be considered an excellent alternative light source owing to its low risk level and energy consumption. A higher dye concentration increases dye absorption on nanoparticles and the occupation of active sites on their surface. Additionally, dye molecules absorb more UV energy with a higher dye concentration, which reduces dye degradation. Similar results have been found by Daneshvar et al. (2003).

3.2.4. Photocatalytic effect of α-Fe_2O_3/WO_3 under two light sources

In this study, the solution of magnetic α-Fe_2O_3/WO_3 was mixed with RB19 in different dye concentrations of 10, 30, 50 and 70 mg/L. The concentration of the nanophotocatalyst was 1 g/L, and the pH was fixed at 2. The photocatalytic process was conducted under two light sources (UV-C and visible LED lamps). Fig. 11 shows the experimental results. In comparison with WO_3/NaOH, α-Fe_2O_3/WO_3 was more reactive to removal of dye concentration. The removal efficiencies for 10, 30, 50, and 70 mg/L of RB19 solution were approximately 100%, 91%, 77%, and 62%, respectively, for 240-min radiation under UV-C light. On the other hand, the 360-min radiation of LED lamps was effective in removing 100%, 70%, 44%, and 27% of RB19 for dye concentrations of 10, 30, 50, and 70 mg/L, respectively.

The mixture of WO_3 with α-Fe_2O_3 consumed excited electrons much more easily than the mixture of WO_3 with NaOH. A greater consumption rate decreased the recombination of photogenerated electron−hole pairs in a semiconductor. In recent years, magnetic materials have been widely developed because of their synergistic effects in photocatalytic degradation. In fact, the coupled structure of hematite and WO_3 can stop the recombination of electrons on the surface of semiconductors. Due to this coupled structure, electrons and holes are transferred to the surface of α-Fe_2O_3 and the semiconductor, enhancing the photodegradation efficiency by forming nonselective ·OH radicals with less recombination of electrons and holes. This can introduce

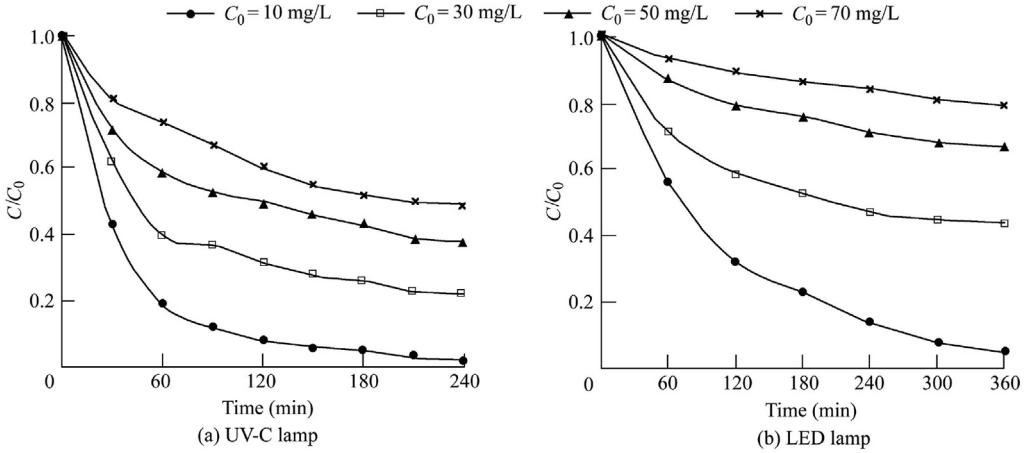

Fig. 10. Effect of initial concentration of RB19 and irradiation on ratio of residual color to initial color (with initial pH of 2 and WO_3/NaOH dosage of 1 g/L).

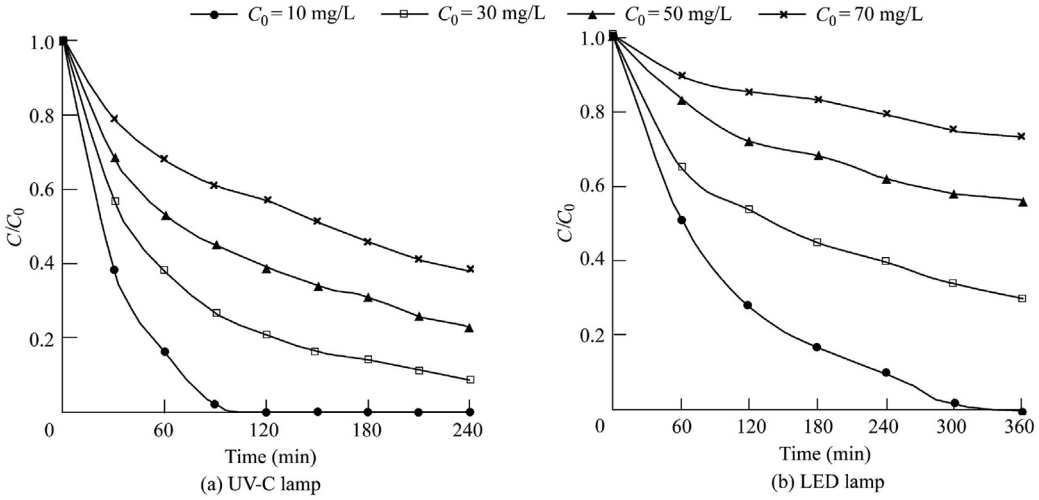

Fig. 11. Effect of initial concentration of dye and irradiation on ratio of residual color to initial color (with initial pH of 2 and α-Fe_2O_3/WO_3 dosage of 1 g/L).

more radicals on the surface of the semiconductor, thereby decomposing all types of organic pollutants including dyes. Fig. 12 shows the contribution of α-Fe_2O_3 and WO_3 to the improvement of degradation efficiency. Another positive effect is the appearance of Fe^{2+} ions on the surface of the semiconductor, which act as a trap for holes and electrons and therefore prevent recombination in the degradation process.

Fig. 13 displays the different performances of α-Fe_2O_3/WO_3 and WO_3/NaOH in removing RB19 with various dye concentrations. The effects of UV and LED light sources were compared as well. The UV lamps had higher penetration and intensity, leading to a more effective degradation process. By contrast, the LED lamps were also effective and properly decomposed the dye compounds, with a degradation rate of 100% after 360 min. It should be noted that, under specific conditions with optimum factors, dye removal was tested with α-Fe_2O_3/WO_3 for 400 min under the exposure of LED visible light. The results showed that the pollutant removal with visible light became steady after 360 min, and 100% of dyes were degraded. Thus, compared with the dangerous and less environmentally friendly UV lamps, visible light allowed for substantially more dye removal with magnetic tungsten photocatalysts.

3.2.5. *Effect of photocatalytic activity on organic matter*

Further experiments were conducted to evaluate the effectiveness of photocatalytic activity in removing organic matter such as chemical oxygen demand (COD) in optimum operating conditions (with α-Fe_2O_3/WO_3 dosage of 1 g/L and pH of 2) and different initial dye concentrations (10, 30, 50, and 70 mg/L). The initial COD-equivalent dye solution dosages were 12.6, 38.1, 62.8, and 87.5 mg/L, respectively. Fig. 14 shows that the COD removal efficiency basically showed a similar oscillatory trend for different pollutant concentrations. In the first 60 min, the COD removal efficiency increased. In the period of 60−90 min, the removal

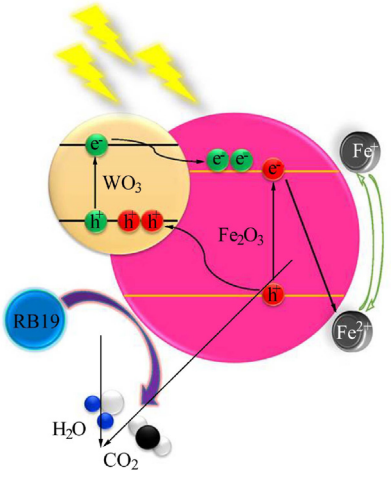

Fig. 12. Effect of coupled structure on photodegradation efficiency.

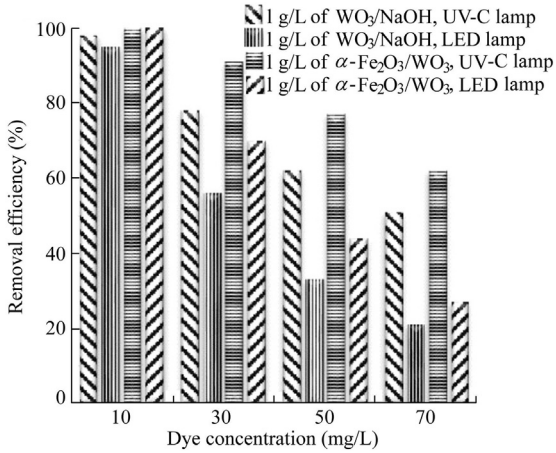

Fig. 13. Comparison between dye removal efficiencies of α-Fe_2O_3/WO_3 and WO_3/NaOH with various RB19 concentrations.

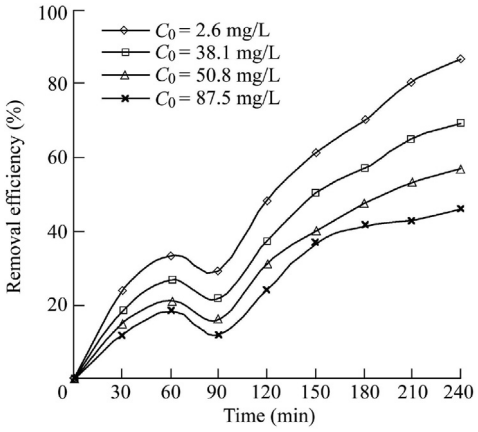

Fig. 14. Removal efficiency of COD (with α-Fe_2O_3/WO_3 dosage of 1 g/L and pH of 2).

efficiency substantially declined. The COD removal process then continued to the end of the reaction. For example, in the case with an initial COD concentration of 38.1 mg/L, the removal efficiency was merely 27% in the first 60 min, and it reached 21.5% with a 5% reduction in the next 30 min. During the remaining irradiation time, the reactor performance gradually improved, and the COD removal efficiency ultimately reached 69.5%. Throughout the process, the highest removal efficiency was 87% for an initial COD concentration of 12.6 mg/L. Comparatively, the reactor exhibited a greater efficiency in removing the dye solution than in removing COD. The main reason is related to the dye process. In fact, the dye chemical structures turn into intermediate compounds resulting from break down of the dye chemical structure and the subsequent recombination of these fragments to form new materials. The reason for the fluctuation in the COD removal efficiency over the test period is the production of these intermediate products.

3.3. Reusability of α-Fe_2O_3/WO_3

Due to the magnetic behavior of α-Fe_2O_3/WO_3 nanoparticles, it is much easier to reuse these nanoparticles. An external magnetic field can be used to separate all nanophotocatalysts from absorbed dyes for use in the next cycle. In this study, a certain amount of dye was mixed with the nanophotocatalyst in order to measure the photodegradation efficiency. After each step, the dye solution was adjusted to the initial concentration, and the recovered magnetic photocatalyst was subsequently added for the next cycle. The results showed that the removal efficiencies of cycles 1, 2, 3, 4, 5, and 6 are 100%, 100%, 98%, 95%, 94%, and 93%, respectively. After six cycles, the degradation efficiency of the nanophotocatalyst decreased by 7%. This efficiency decline may be attributed to the reduction of the active area on the surface of nanophotocatalysts because many dye molecules on the nanoparticles or nanophotocatalysts escaped during sampling.

4. Conclusions

In this study, the photocatalytic degradation of RB19 was investigated in a slurry system using UV and LED lamps as light sources and using α-Fe_2O_3/WO_3 and WO_3/NaOH as photocatalysts. The effects of different parameters including irradiation time, initial concentration of RB19, nanophotocatalyst dosage, and pH were examined. Meanwhile, the magnetic nanophotocatalyst was also characterized. The main conclusions are as follows:

(1) α-Fe_2O_3/WO_3 magnetic nanoparticles had a strong photocatalytic ability in terms of RB19 degradation. Increasing the number of nanoparticles to a certain amount increased the removal efficiency, but the efficiency of the system mostly decreased.

(2) Coupling the structure of the magnetic nanophotocatalyst significantly aids in preventing recombination of electron−hole pairs on the surface of the nanophotocatalyst.

(3) The removal efficiency of the system under LED visible light was high over a longer period of time and decomposed almost 100% of the dye solution. LED visible lights improved the degradation process and increased the efficiency for longer time periods, showing similarity to the performance of UV lamps. This indicates that LED visible lamps are promising for applications in practical cases on an industrial scale. In addition, they are more environmentally friendly than UV lights. This trait requires more attention in further studies.

(4) In comparison with the common photocatalyst (WO_3/NaOH), the new magnetic photocatalyst α-Fe_2O_3/WO_3 showed a better performance under irradiation from both light sources. The magnetic separation process facilitated the reusability of magnetic materials. The RB19 removal efficiency merely decreased by 7% after the magnetic α-Fe_2O_3/WO_3 photocatalyst was used for six cycles.

Declaration of competing interest

The authors declare no conflicts of interest.

References

Abbasi Asl, E., Haghighi, M., Talati, A., 2020. Enhanced simulated sunlight-driven magnetic $MgAl_2O_4$-AC nanophotocatalyst for efficient degradation of organic dyes. Separ. Purif. Technol. 251, 117003. https://doi.org/10.1016/j.seppur.2020.117003.

Akyol, A., Bayramoğlu, M., 2005. Photocatalytic degradation of Remazol Red F3B using ZnO catalyst. J. Hazard Mater. 124(1), 241−246. https://doi.org/10.1016/j.jhazmat.2005.05.006.

Al-Ani, Y., Li, Y., 2012. Degradation of C.I. reactive blue 19 using combined iron scrap process and coagulation/flocculation by a novel $Al(OH)_3$-polyacrylamide hybrid polymer. J. Taiwan Inst. Chem. Eng. 43(6), 942−947. https://doi.org/10.1016/j.jtice.2012.07.005.

Banić, N.D., Abramović, B.F., Krstić, J.B., Šojić Merkulov, D.V., Finčur, N.L., Mitrić, M.N., 2019. Novel WO_3/Fe_3O_4 magnetic photocatalysts: Preparation, characterization and thiacloprid photodegradation. J. Ind. Eng. Chem. 70, 264−275. https://doi.org/10.1016/j.jiec.2018.10.025.

Bel Hadjltaief, H., Galvez, M.E., Ben Zina, M., da Costa, P., 2019. TiO_2/clay as a heterogeneous catalyst in photocatalytic/photochemical oxidation of

anionic reactive blue 19. Arabian J. Chem. 12(7), 1454−1462. https://doi.org/10.1016/j.arabjc.2014.11.006.

Chen, J., Poon, C.-S., 2009. Photocatalytic activity of titanium dioxide modified concrete materials: Influence of utilizing recycled glass cullets as aggregates. J. Environ. Manag. 90(11), 3436−3442. https://doi.org/10.1016/j.jenvman.2009.05.029.

Daneshvar, N., Salari, D., Khataee, A.R., 2003. Photocatalytic degradation of azo dye acid red 14 in water: Investigation of the effect of operational parameters. J. Photochem. Photobiol. Chem. 157(1), 111−116. https://doi.org/10.1016/S1010-6030(03)00015-7.

Daneshvar, N., Salari, D., Khataee, A.R., 2004. Photocatalytic degradation of azo dye acid red 14 in water on ZnO as an alternative catalyst to TiO_2. J. Photochem. Photobiol. Chem. 162(2), 317−322. https://doi.org/10.1016/S1010-6030(03)00378-2.

Gómez-Pastora, J., Dominguez, S., Bringas, E., Rivero, M.J., Ortiz, I., Dionysiou, D.D., 2017. Review and perspectives on the use of magnetic nanophotocatalysts (MNPCs) in water treatment. Chem. Eng. J. 310, 407−427. https://doi.org/10.1016/j.cej.2016.04.140.

Guimarães, J.R., Guedes Maniero, M., Nogueira de Araújo, R., 2012. A comparative study on the degradation of RB-19 dye in an aqueous medium by advanced oxidation processes. J. Environ. Manag. 110, 33−39. https://doi.org/10.1016/j.jenvman.2012.05.020.

Han, F.G., Li, H.P., Fu, L., Yang, J., Liu, Z., 2016. Synthesis of S-doped WO_3 nanowires with enhanced photocatalytic performance towards dye degradation. Chem. Phys. Lett. 651, 183−187. https://doi.org/10.1016/j.cplett.2016.03.017.

Hitkari, G., Singh, S., Pandey, G., 2018. Photoluminescence behavior and visible light photocatalytic activity of ZnO, ZnO/ZnS and ZnO/ZnS/α-Fe_2O_3 nanocomposites. Trans. Nonferrous Metals Soc. China 28(7), 1386−1396. https://doi.org/10.1016/S1003-6326(18)64777-6.

Hong, L., Liu, X.M., Tan, L., Cui, Z.D., Yang, X.J., Liang, Y.Q., Li, Z.Y., Zhu, S.L., Zheng, Y.F., Yeung, K.W.K., et al., 2019. Rapid biofilm elimination on bone implants using near-infrared-activated inorganic semiconductor heterostructures. Adv. Healthcare Mater. 8(19), 1900835. https://doi.org/10.1002/adhm.201900835.

Hosseini, S., Eftekhari, E., Soltani, S., Eghbali Babadi, F., Jeffery Minggu, L., Ismail, M.H.S., 2014. Synthesis, characterization and performance evaluation of three-layered photoanodes by introducing a blend of WO_3 and Fe_2O_3 for dye degradation. Appl. Surf. Sci. 289, 53−61. https://10.1016/j.apsusc.2013.10.089.

Kabra, A.N., Khandare, R.V., Govindwar, S.P., 2013. Development of a bioreactor for remediation of textile effluent and dye mixture: A plant-bacterial synergistic strategy. Water Res. 47(3), 1035−1048. https://doi.org/10.1016/j.watres.2012.11.007.

Kako, T., Meng, X., Ye, J., 2014. Enhancement of photocatalytic activity for WO_3 by simple NaOH loading. Appl. Catal. Gen. 488, 183−188. https://doi.org/10.1016/j.apcata.2014.09.046.

Kansal, S.K., Singh, M., Sud, D., 2007. Studies on photodegradation of two commercial dyes in aqueous phase using different photocatalysts. J. Hazard Mater. 141(3), 581−590. https://doi.org/10.1016/j.jhazmat.2006.07.035.

Karimi, H., Rajabi, H.R., Kavoshi, L., 2020. Application of decorated magnetic nanophotocatalysts for efficient photodegradation of organic dye: A comparison study on photocatalytic activity of magnetic zinc sulfide and graphene quantum dots. J. Photochem. Photobiol. Chem. 397, 112534. https://doi.org/10.1016/j.jphotochem.2020.112534.

Li, Y., Feng, J., Li, H., Wei, X., Wang, R., Zhou, A., 2016. Photoelectrochemical splitting of natural seawater with α-Fe_2O_3/WO_3 nanorod arrays. Int. J. Hydrogen Energy 41(7), 4096−4105. https://doi.org/10.1016/j.ijhydene.2016.01.027.

Lourenço, N.D., Franca, R.D.G., Moreira, M.A., Gil, F.N., Viegas, C.A., Pinheiro, H.M., 2015. Comparing aerobic granular sludge and flocculent sequencing batch reactor technologies for textile wastewater treatment. Biochem. Eng. J. 104, 57−63. https://doi.org/10.1016/j.bej.2015.04.025.

Manceriu, L., Carcel, R.A., 2011. Prediction of TiO_2 and WO_3 nanopowders surface charge by the evaluation of point of zero charge (PZC). Environ. Eng. Manag. J. 10(8), 1021−1026. https://10.30638/eemj.2011.148.

Marcucci, M., Nosenzo, G., Capannelli, G., Ciabatti, I., Corrieri, D., Ciardelli, G., 2001. Treatment and reuse of textile effluents based on new ultrafiltration and other membrane technologies. Desalination 138(1), 75−82. https://doi.org/10.1016/S0011-9164(01)00247-8.

Mkhalid, I.A., 2016. Photocatalytic degradation of herbicides under visible light using Pd-WO_3 nanorods. Ceram. Int. 42(14), 15975−15980. https://doi.org/10.1016/j.ceramint.2016.07.100.

Mu, W.J., Yu, Q.H., Li, X.L., Wei, H.Y., Jian, Y., 2017. Efficient removal of Cs^+ and Sr^{2+} from aqueous solution using hierarchically structured hexagonal tungsten trioxide coated Fe_3O_4. Chem. Eng. J. 319, 170−178. https://doi.org/10.1016/j.cej.2017.02.153.

Parthibavarman, M., Karthik, M., Prabhakaran, S., 2018. Facile and one step synthesis of WO_3 nanorods and nanosheets as an efficient photocatalyst and humidity sensing material. Vacuum 155, 224−232. https://doi.org/10.1016/j.vacuum.2018.06.021.

Pirkarami, A., Olya, M.E., 2017. Removal of dye from industrial wastewater with an emphasis on improving economic efficiency and degradation mechanism. J. Saudi Chem. Soc. 21(s1), S179−S186. https://doi.org/10.1016/j.jscs.2013.12.008.

Serrà, A., Pip, P., Gómez, E., Philippe, L., 2020. Efficient magnetic hybrid ZnO-based photocatalysts for visible-light-driven removal of toxic cyanobacteria blooms and cyanotoxins. Appl. Catal. B Environ. 268, 118745. https://doi.org/10.1016/j.apcatb.2020.118745.

Wang, H.X., Wang, C.H., Cui, X.M., Qin, L., Ding, R.M., Wang, L.C., Liu, Z., Zheng, Z.F., Lv, B.L., 2018. Design and facile one-step synthesis of $FeWO_4$/Fe_2O_3 di-modified WO_3 with super high photocatalytic activity toward degradation of quasi-phenothiazine dyes. Appl. Catal. B Environ. 221, 169−178. https://doi.org/10.1016/j.apcatb.2017.09.011.

Xue, D., Zong, F., Zhang, J., Lin, X., Li, Q., 2019. Synthesis of Fe_2O_3/WO_3 nanocomposites with enhanced sensing performance to acetone. Chem. Phys. Lett. 716, 61−68. https://doi.org/10.1016/j.cplett.2018.12.016.

Yurtsever, A., Çınar, Ö., Sahinkaya, E., 2016. Treatment of textile wastewater using sequential sulfate-reducing anaerobic and sulfide-oxidizing aerobic membrane bioreactors. J. Membr. Sci. 511, 228−237. https://doi.org/10.1016/j.memsci.2016.03.044.

Zhang, X.C., Tang, A.D., Jia, Y.R., Wang, Y.T., Wang, H.X., Zhang, S.Y., 2017. Enhanced visible-light-driven photocatalytic performance of Ag/$AgGaO_2$ metal semiconductor heterostructures. J. Alloys Compd. 701, 16−22. https://doi.org/10.1016/j.jallcom.2017.01.085.